Synthesis and Characterization of Discrete Luminescent Erbium-Doped Silicon Nanocrystals

John St. John,[†] Jeffery L. Coffer,*[,†] Yandong Chen,[‡] and Russell F. Pinizzotto*[,‡]

Contribution from the Department of Chemistry, Texas Christian University, Fort Worth, Texas, 76129, and Materials Science Department, University of North Texas, Denton, Texas 76203

Received August 10, 1998

Abstract: The preparation of discrete erbium-doped silicon nanoparticles prepared by the co-pyrolysis of disilane and the volatile complex $Er(tmhd)_3$ (tmhd = 2,2,6,6-tetramethyl-3,5-heptanedionato) is described. The nanoparticles were characterized by transmission electron microscopy, selected area electron diffraction, X-ray dispersive spectroscopy, photoluminescence, and UV−visible absorption spectroscopies. Erbium-doped silicon nanoparticles possess a distinctive dark contrast in the transmission electron microscope, and the presence of erbium is confirmed by X-ray energy dispersive spectroscopy. The mean diameter of the nanoparticle aggregates can be shifted by altering the length of the pyrolysis oven employed. Chacteristic Er^{3+} near-infrared photoluminescence at 1540 nm is detected in these doped nanoparticles; preliminary excitation and power dependence measurements of this luminescence suggest a carrier-mediated emission mechanism.

Silicon, the semiconductor of choice for existing electronic technologies, faces formidable challenges in future integration with optoelectronic devices.[1] Two strategies designed to thwart its intrinsic indirect band gap and the accompanying absence of efficient light emission are (1) the formation of luminescent nanophase Si[2,3] and (2) rare earth incorporation into single-crystal Si.[4−7] The rare earth ion erbium is of particular interest for the latter approach because its $(^4I_{13/2}) \rightarrow (^4I_{15/2})$ luminescent transition at 1.54 μm lies at a transmission maximum for silica-based waveguides.[4−8] Until now, however, such studies have been mainly restricted to erbium implanted into bulk Si[8] or porous Si,[9] or alternatively the co-deposition of erbium and silicon thin films.[10] Hence, it has not been possible to explore the effects of rare earth doping of isolated, spherical Si nanoparticles (Scheme 1). The effects of confining *doped* Si in all three dimensions are crucial to the development of Si-based nanophotonics and are of increasing importance as the sizes of individual Si device structures diminish to the nanometer regime.We describe here for the first time the preparation of discrete erbium-doped silicon nanoparticles prepared by the co-pyrolysis of disilane and the volatile complex $Er(tmhd)_3$ (tmhd = 2,2,6,6-tetramethyl-3,5-heptanedionato). The nanoparticles are characterized by transmission electron microscopy (TEM, HREM), selected area electron diffraction, X-ray energy dispersive spectroscopy (XEDS), photoluminescence (PL), and UV−visible absorption spectroscopies.

Scheme 1

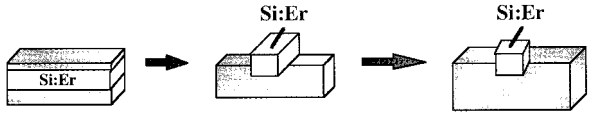

Common routes for the preparation of homogeneous Si nanoparticles include the laser ablation of solid crystalline Si,[10,11] the gas-phase pyrolysis of silane or disilane,[12−15] and the reduction of halosilanes.[16] Our strategy for the preparation of rare earth-doped nanoparticles involves a modification of a high-temperature aerosol reaction involving the combustion of disilane (Si_2H_6, diluted in He carrier gas) followed by oxidation and isolation as a colloidal solution.[12,13] Our apparatus is capable of producing homogeneous oxide-capped Si nanoclusters and also possesses the ability to introduce an additional vapor phase reactant into the reactant stream (Scheme 2).

We employ the known erbium CVD precursor $Er(tmhd)_3$ (tmhd = 2,2,6,6 tetramethyl-3,5-heptanedionato) as the Er source

* Author to whom correspondence should be addressed. e-mail: j.coffer@tcu.edu.

† Texas Christian University.

‡ University of North Texas.

(1) Iyer, S.; Xie, Y.-H *Science* **1993**, *260*, 40.

(2) Canham, L. *Appl. Phys. Lett.* **1990**, *57*, 1046.

(3) For an extensive complilation of fundamental and applied research concerning porous silicon, see: *Properties of Porous Silicon*; Leigh Canham, Ed., EMIS Datareviews Series, INSPEC/IEE Press: U.K., 1997.

(4) Ennen, H.; Schneider, J.; Pomrenke, G.; Axmann, A. *Appl. Phys. Lett.* **1983**, *90*, 943.

(5) Ennen, H.; Pomrenke, G.; Axmann, A.; Eisele, K,; Haydl, W.; Schneider, J. *Appl. Phys. Lett.* **1985**, *46*, 381.

(6) Benton, J. L.; Michel, J.; Kimerling, L. C.; Jacobson, D. C.; Xie, Y.-H.; Eaglesham, D. J.; Fitzgerald, E. A.; Poate, J. M. *J. Appl. Phys.* **1991**, *70*, 2667.

(7) Adler, D. L.; Jacobsen, D. C.; Eaglesham, D. J.; Marcus, M. A.; Benton, J. L.; Poate, J. M.; Citrin, P. H. *Appl. Phys. Lett.* **1992**, *61*, 2181.

(8) Polman, A. *J. Appl. Phys.* **1997**, *82*, 1.

(9) (a) Namavar, F.; Lu, F.; Perry, C. H.; Cremins, A.; Kalkhoran, N.; Soref, R. *J. Appl. Phys.* **1995**, *77*, 4813. (b) Hömmerich, U.; Namavar, F.; Cremins, A.; Bray, K. *Appl. Phys. Lett.* **1996**, *68*, 1951. (c) Tsybeskov, L.; Duttagupta, S.; Hirschman, K.; Fauchet, P.; Moore, K.; Hall, D. *Appl. Phys. Lett.* **1997**, *70*, 1790.

(10) Thilderkvist, A.; Michel, J.; Ngiam, S.; Kimerling, L.; Kolenbrander, K. *Mater. Res. Soc. Symp. Proc.* **1995**, *405*, 265.

(11) Werwa, E.; Seraphin, A. A.; Chiu, L. A.; Zhou, C.; Kolenbrander, K. D. *Appl. Phys. Lett.* **1994**, *64*, 1821.

(12) Littau, K.; Szajowski, P.; Muller, A.; Kortan, A.; Brus, L. *J. Phys. Chem.* **1993**, *97*, 1224.

(13) Brus, L.; Szajowski, P.; Wilson, W.; Harris, T.; Schupler, S.; Citrin, P. *J. Am. Chem. Soc.* **1995**, *117*, 2915.

(14) Wilson, W. L.; Szajowski, P. F.; Brus, L. E. *Science* **1993**, *262*, 1242.

(15) Murthy, T.; Miyamoto, N.; Shibo, M.; Nishizawa, J. *J. Cryst. Growth* **1976**, *33*, 1.

(16) Bley, R. A.; Kauzlarich, S. *J. Am. Chem. Soc.* **1996**, *118*, 12461.

10.1021/ja982838g CCC: $18.00
Published on Web 02/19/1999

Scheme 2

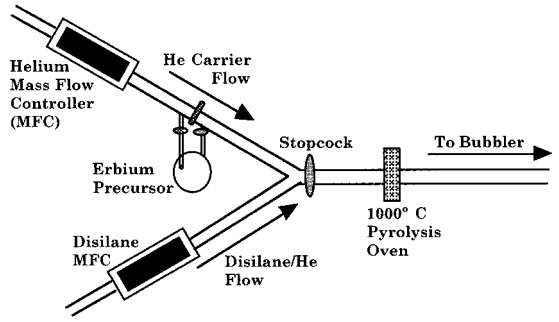

in this reactor. Our initial experiments have focused on the effects of varying the pyrolysis oven length (from 1.5 to 6 cm) on the structure and spectroscopic properties of the nanoparticles isolated from these reaction products.

Experimental Section

Nanoparticle Synthesis. The reactor is constructed from 7 mm i.d. quartz tubing, with gas flow regulated by mass-flow controllers (MKS Inc.). A small pyrolysis oven operating at 1000 °C is located approximately 10 cm from the point where the disilane/He (0.48% Si_2H_6, diluted in He carrier gas (Praxair) at various flow rates (vide supra)) and $Er(tmhd)_3$ (Strem, Inc.)/He (Praxair, UHP grade, maintained at a flow rate of 3000 sccm) initially mix. After pyrolysis, the reaction mixture travels downstream to a dual bubbler system where the aerosol is collected as an ethylene glycol colloid. At the end of a 24 h reaction period, the reaction mixture consists of a yellow colloid and brown solid. After initial separation by centrifugation, the supernatant is treated with THF in a ratio of 15:1 (THF:ethylene glycol) to force precipitation of a solid product. The product is washed several times with ethanol to remove physisorbed erbium ions. This precipitate can be redissolved in ethylene glycol or acetone.

Instrumentation. Structural characterization of Er^{3+}-doped Si nanocrystal aggregates was performed using a JEOL 200CX TEM at the University of North Texas. Samples were deposited on carbon films on copper grids, and the ethylene glycol was allowed to evaporate prior to imaging. Structural characterization of individual Er^{3+}-doped Si nanocrystals by HREM was performed using a Hitachi H9000 TEM at UNT. X-ray energy dispersive spectroscopy (XEDS) analyses of Er^{3+}-doped Si aggregates were performed in the scanning transmission electron microscopy (STEM) mode of the JEOL 200CX. Selected area electron diffraction patterns (SADP) were obtained during TEM analyses. UV−visible spectra were obtained using a Hewlett-Packard 8452A diode array spectrometer. Low-resolution (±4 nm) near-IR photoluminescence (PL) spectra were obtained using an Applied Detector Corp. liquid N_2-cooled Ge detector in conjunction with a Stanford Research Systems Chopper/Lock-in amplifier and an Acton Research Corp. 0.25 m monochromator. Excitation was provided by a Coherent Ar^+ laser. A 10 cm lens was used to focus light emitted from the samples onto the monochromator entrance slit. Emitted light was collected at 90° relative to the excitation direction. A 1000 nm cutoff filter (Melles Griot) was positioned over the monochromator entrance slit to filter out second- and third-order light.

Results and Discussion

A conventional bright-field transmission electron micrograph of a sample collected from the 3.0 cm long reaction furnace is shown in Figure 1. There are two types of material clearly visible in this micrograph with either light contrast (L) or dark contrast areas (D). Selected area electron diffraction patterns (SADP) from both areas are consistent with the diamond-cubic phase of silicon. There is no evidence of elemental Er, Er silicide, or Er oxide phases.

X-ray energy dispersive spectroscopy (XEDS) analyses of the light and dark contrast areas were performed in the scanning transmission electron microscopy (STEM) mode (Figure 2). For dark contrast areas such as D in Figure 1, the spectra indicate Si, and most importantly, the Er-L and Er-M peaks at 6.9 and 1.4 keV, respectively (Figure 2a). An estimated Er concentration of 2−3% is based on quantitative analyses of the spectra. Similar SADP and XEDS results were found for samples generated using all three reaction furnace lengths. There is no evidence

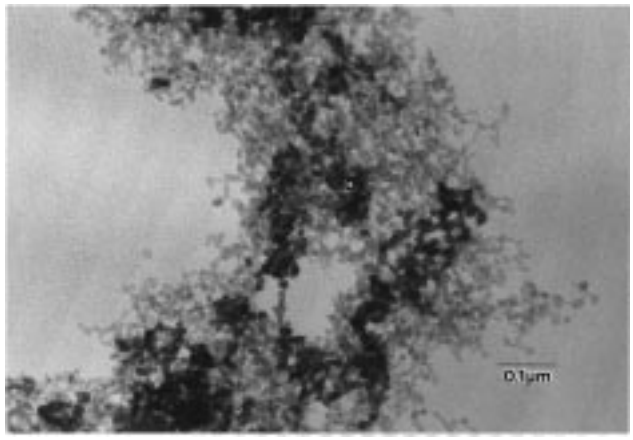

Figure 1. Conventional bright-field transmission electron micrograph of a sample collected from the 3.0 cm long reaction furnace. There are two distinct morphologies with light (L) and dark (D) contrast. The dark contrast areas contain Er while the light contrast areas do not.

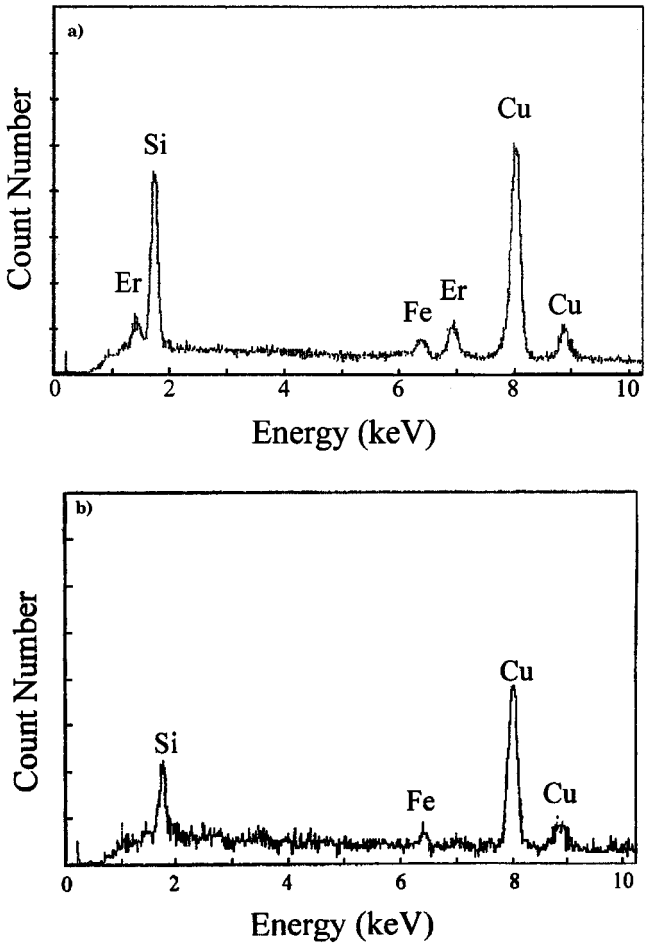

Figure 2. X-ray energy dispersive spectra from (a) a dark contrast area similar to D and (b) a light contrast area similar to L in Figure 1. The Cu is from the instrument and the Cu grid used to support the TEM sample; the Fe is an artifact from the XEDS system.

Table 1. Statistical Data for Er-Doped Si Nanostructure Size versus Reaction Furnace Length

reaction furnace length (cm)	ave struct size[a] linear statistics (nm)	std dev (linear statistics)	ave struct size log-normal statistics (nm)	std dev (log-normal statistics)
1.5	11.3	3.8	1.03	0.14
3.0	13.8	4.8	1.11	0.15
6.0	15.2	6.6	1.15	0.16

[a] The average structure sizes were determined by measuring 400−700 individual structure diameters for each type of sample.

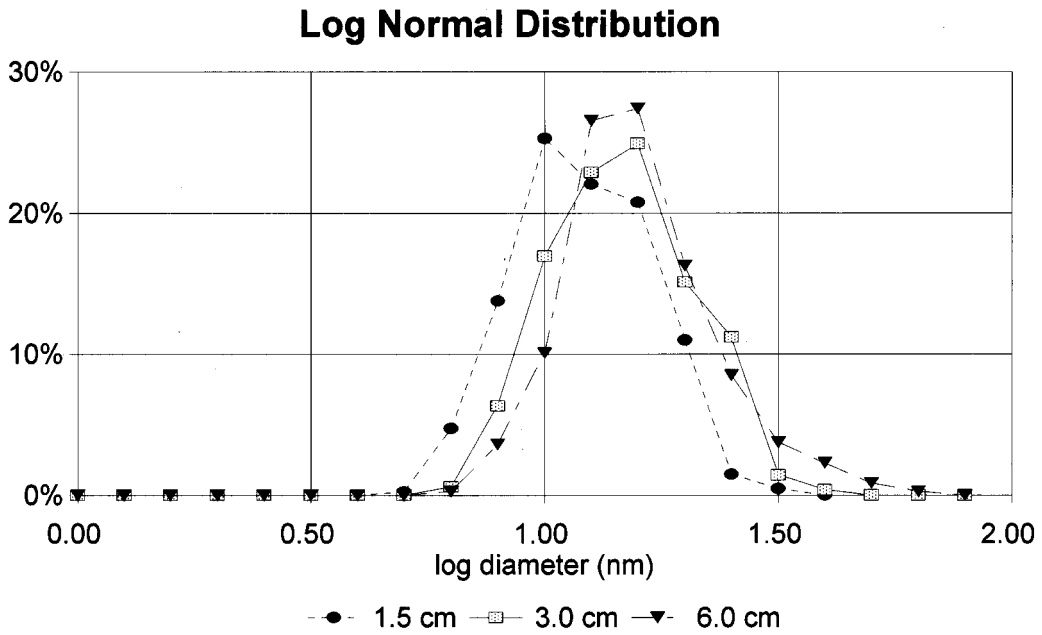

Figure 3. Log-normal structure size distributions for samples from the 1.5, 3.0, and 6.0 cm reaction furnaces.

of Er in the light contrast areas similar to L in Figure 1 (Figure 2b), or in control samples prepared without $Er(tmhd)_3$.

The average structure size of the features visible in Figure 1 was determined by measuring 400−700 individual structure diameters for each type of sample. The averages and standard deviations for samples isolated from all three reaction furnace lengths are presented in Table 1. The structure sizes are best described using log-normal statistics, as is usual for structures formed by agglomeration or diffusion-controlled growth.[17] The average structure size and standard deviation both increase with increasing furnace length, from an average size of 11 nm for the 1.5 cm oven to 15 nm for the 6.0 cm oven. However, the size distributions have significant overlaps (Figure 3). To test whether the distributions were each a sample of a single distribution or from separate distributions, Student's t-tests were performed. The t-statistic in all cases is less than 2.2×10^{-7}, meaning that there are three distinct sample distributions and not three measurements of a single distribution, with a high degree of statistical significance.

High-resolution transmission electron microscopy (HREM) was performed to elucidate the structure of the two types of material observed by CTEM and to try to determine the location of the Er incorporated into the samples. Figure 4 is a high-magnification HREM view of one of the dark contrast structures from the 3.0 cm furnace system observed by CTEM. Each dark contrast structure is an aggregate composed of numerous discrete Si nanoparticles, each nanoparticle with a mean diameter of 3 nm. Many of the particles contain various types of defects such as edge dislocations and stacking faults (Figure 4b). There is no evidence of Er clustering or second phase formation in any of the HREM micrographs obtained to date. The inclusion of Er in the Si lattice may be responsible for some of the defect formation. However, we have synthesized control samples of homogeneous Si nanoparticles produced by disilane pyrolysis with a 3.0 cm oven in the absence of the $Er(tmhd)_3$ complex, and numerous stacking faults and other defects are clearly present in the control nanoparticles (Figure 5). It is important to stress, though, that there is a clear structural difference induced by the Er^{3+} in the doped nanoparticles, as the diffraction rings in the SADP patterns obtained from Si nanoparticles containing Er are significantly broader than those obtained from nanoparticles composed of Si alone. This is additional evidence that Er incorporation enhances defect formation within the Si nanoparticles (Figure 6).

A typical UV/visible absorption spectrum of an Er-doped Si nanoparticle sample with a mean particle size of 2.5 nm dissolved in ethylene glycol reveals a broad absorption tail with an onset of absorption near 600 nm (Figure 7a). This behavior is consistent with that of a solution of indirect band gap Si nanoparticles.[12]

The room-temperature photoluminescence has also been measured. Upon excitation at 488 nm, the anticipated Er^{3+} emission maximum near 1.54 μm, associated with the $(^4I_{13/2}) \rightarrow (^4I_{15/2})$ transition, is observed (Figure 7b). Two scenarios are possible for the fundamental luminescence mechanism of the Er^{3+} centers:[8] (1) Si carrier-mediated excitation of the Er centers by energy transfer (as in ion-implanted single-crystal Si) or (2) direct absorption into energy levels associated with the Er centers (as in Er-doped SiO_2 and silicate glasses). The first mechanism is operative in the case of erbium ions which are implanted into single-crystal Si, whereby a Si exciton engages

(17) (a) Granqvist, C. G.; Buhrman, R. *J. Appl. Phys.* **1976**, *47*, 2200. (b) Granqvist, C. G.; Buhrman, R. *Appl. Phys. Lett.* **1975**, *27*, 693. (c) Coffer, J. L.; Bigham, S. R.; Pinizzotto, R. F.; Yang, H. *Nanotechnology* **1992**, *3*, 69.

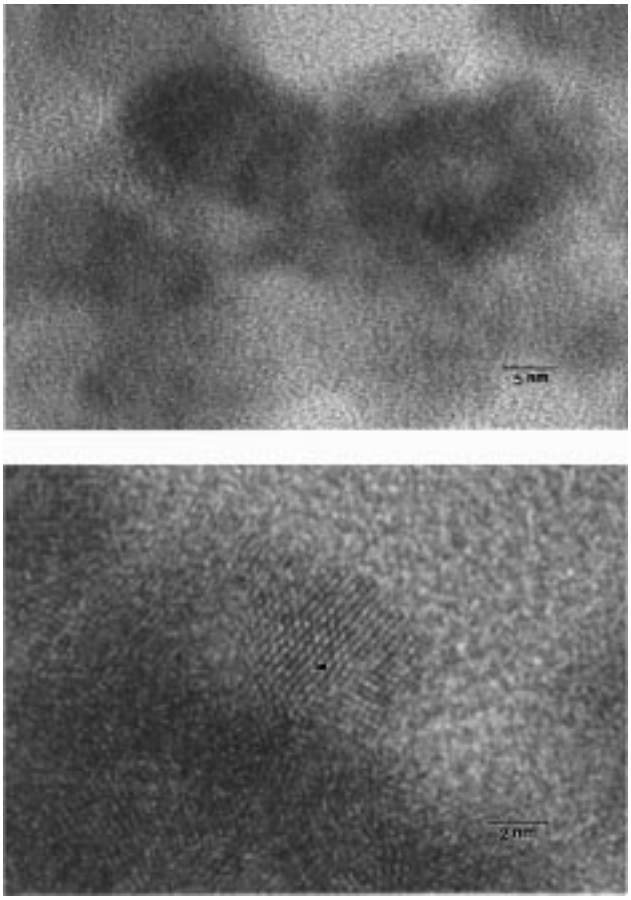

Figure 4. High-resolution electron micrograph of an Er-doped Si nanoparticle prepared from the 3.0 cm long furnace. The dark contrast areas visible in Figure 1 are composed of an agglomeration of nanoparticles. (b) High-resolution electron micrograph of a sample from the 3.0 cm long furnace showing the presence of an edge dislocation (indicated by the arrow).

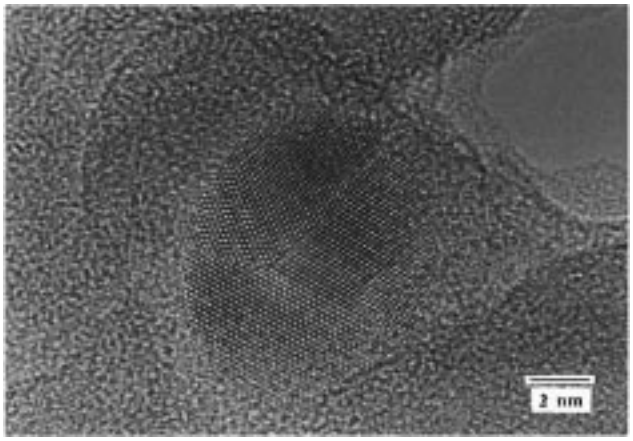

Figure 5. High-resolution electron micrograph of a control sample of homogeneous Si nanoparticles produced by disilane pyrolysis with a 3.0 cm oven in the absence of the $Er(tmhd)_3$ complex. This particular nanocrystal appears to be twinned, with stacking faults and other defects visible in this image.

in energy transfer with the Er to produce the near-infrared emission (Scheme 3).

The second scenario is dominant in systems such as Er-doped SiO_2 and silicate glasses, where excitation at 488 nm results in the population of the $^4F_{7/2}$ level. An electron in this level can undergo nonradiative decay into the $^4I_{13/2}$ level, leading to the fluorescence transition to the $^4I_{15/2}$ level at approximately 1540 nm.

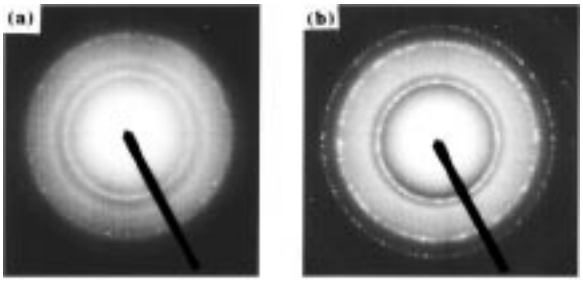

Figure 6. Selected area diffraction patterns of (a) Er-doped Si nanoparticles prepared from the 3.0 cm long furnace and (b) control sample of homogeneous Si nanoparticles produced by disilane pyrolysis with a 3.0 cm oven in the absence of the $Er(tmhd)_3$ complex.

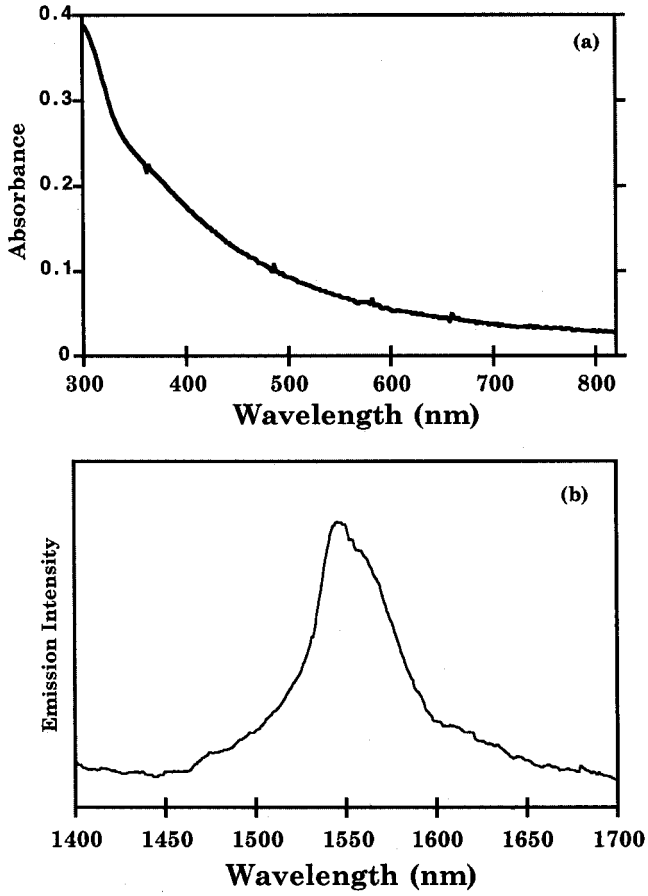

Figure 7. (a) Room-temperature visible absorption spectrum of Er-doped Si nanoparticles in ethylene glycol solution produced from disilane pyrolysis (3.2 sccm) in a 3.0 cm furnace. (b) Room-temperature photoluminescence spectrum of Er-doped Si nanoparticles in ethylene glycol solution produced from disilane pyrolysis (3.2 sccm) in a 3.0 cm furnace, demonstrating the near-infrared emission near 1540 nm ($\lambda_{ex} = 488$ nm).

To analyze these possibilities, we have carried out measurements of the excitation wavelength and power dependence of the observed 1.54 μm photoluminescence. For an excitation wavelength range of 475−514 nm, we find that there is a monotonic decrease in 1.54 μm emission intensity as the excitation wavelength increases (Figure 8a). No distinct increase in the Er^{3+} PL is observed upon excitation at either 488 or 514 nm; such resonant absorption would be detected if a direct excitation process was indeed responsible. Thus the steady decrease in near-IR PL intensity with increasing excitation wavelength is consistent with a carrier-mediated process.

The near-IR PL intensity is observed to be a sublinear function of the pump laser power for all samples measured

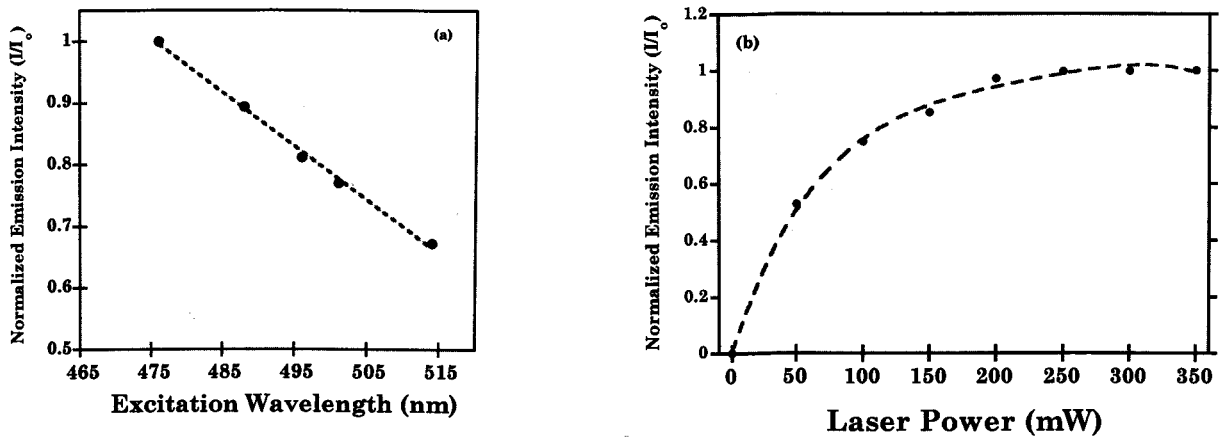

Figure 8. Excitation wavelength (a) and power dependence (b) of the integrated near-infrared PL intensity for Er-doped Si nanoparticles in ethylene glycol solution produced from disilane pyrolysis (3.2 sccm) in a 3.0 cm furnace.

Scheme 3

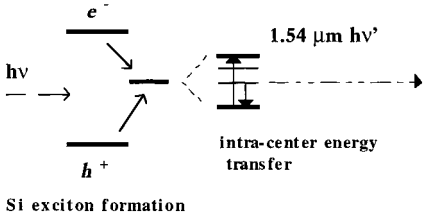

(Figure 8b). This observation is also consistent with a carrier-mediated process, as reported for Er^{3+} in several systems.[9b,19−22] Two mechanisms have been proposed to explain the sublinear power dependency for Er^{3+} in crystalline semiconductors: (1) saturation of optically active Er^{3+} centers with exciting light[8] and (2) an increased contribution from nonradiative Auger quenching processes occurring at excitation saturation levels, as energy from electron/hole recombination is transferred to electrons and then to the surrounding silicon matrix as heat.[19]

It is important to note that for these Er-doped Si nanoparticles, no visible luminescence associated with the Si nanoparticles is detected. In principle, Si nanoparticles approximately 3 nm in diameter are within the realm of kinetic quantum confinement for homogeneous Si nanoparticles, with an anticipated accompanying visible luminescence band.[18] The absence of such visible emission is consistent with energy transfer from the Si exciton to the Er^{3+} centers. However, recall that careful strutiny of the microstructure of control samples of homogeneous Si nanoparticles produced by disilane pyrolysis with a 3.0 cm oven in the absence of the $Er(tmhd)_3$ complex shows that numerous stacking faults and other defects are clearly present, and such defects are also likely candidates for eliminating visible PL in nanoparticles through nonradiative pathways.

The fundamental mechanism of doped nanoparticle formation is without question an extremely complex reaction pathway that has not been elucidated at this point. Despite numerous investigations, the nucleation of homogeneous diamond cubic Si from silylene oligomers produced from silane/disilane pyrolysis is itself not well understood.[22] One proposed mechanistic step suggests that at some point silylsiylene or silylene species are transformed to a crystalline product:

$$Si_nH_{2n+2} + Si_nH_{2n} \rightarrow Si\ (s) \qquad (1)$$

In extrapolating this idea to our system, we speculate that the key question likely entails what critical Si cluster or silylene oligomer size forms prior to association with one or more Er centers:

$$Si_nH_{2n+2}/Si_nH_{2n} + xEr^{3+} \rightarrow \text{Er-doped Si nanoparticles} \qquad (2)$$

A relevant associated question to raise here addresses the extent of particle coalescence and growth after this key step. These issues, along the role of the well-known limited solubility of erbium in silicon,[23] are currently under investigation.

This demonstration of the ability to produce doped nanoscale Si dots with luminescent centers effectively opens the door for the fabrication of a wide variety of rare earth-doped Si nanoparticles, whose emission maximum can be "tuned" by the selection of a particular rare earth ion (ranging from blue emission from Tb^{3+} to near-infrared from Er^{3+}). Such materials are of enormous potential value, for example, in composite films with conducting polymers or other matrices for optical and optoelectronic applications. These and a number of related experiments are in progress.

Acknowledgment. The authors gratefully acknowledge financial support of this research by the Robert A. Welch Foundation (J.L.C.) and a UNT Faculty Research Grant (R.F.P.).

JA982838G

(18) Schuppler, S.; Friedman, S.; Marcus, M.; Adler, D.; Xie, Y.-H.; Ross, F. M.; Harris, T. D.; Brown, W. L., Chabal, Y.; Brus, L.; Citrin, P. *Phys. Rev. Lett.* **1994**, *72*, 2648.

(19) Polman, A.; van den Hoven, G. N.; Cluster, J. S.; Shin, J. H.; Serna, R.; Alkemade, P. F. A. *J. Appl. Phys.* **1995**, *77*, 1256.

(20) Coffa, S.; Franzò, G.; Priolo, F.; Polman, A.; Serna, R. *Phys. Rev. B* **1994**, *49*, 313.

(21) Kimura, T.; Yokoi, A.; Horiguchi, H.; Saito, R.; Ikoma, T.; Sato, A. *Appl. Phys. Lett.* **1994**, *65*, 983.

(22) Giunta, C.; McCurdy, R.; Chapple-Sokol, J.; Gordon, R. *J. Appl. Phys.* **1990**, *67*, 1062.

(23) Ren, F.; Michel, J.; Sun-Paduano, Q.; Zheng, B.; Kitagawa, H.; Jacobson, D. C.; Poate, J. M.; Kimerling, L. C. *Mater. Res. Soc. Symp. Proc.* **1993**, *298*, 415.